

# Point Cloud Pre-training by Mixing and Disentangling

Chao Sun, Zhedong Zheng and Yi Yang, *Senior Member, IEEE*

**Abstract**—The annotation for large-scale point clouds is still time-consuming and unavailable for many real-world tasks. Point cloud pre-training is one potential solution for obtaining a scalable model for fast adaptation. Therefore, in this paper, we investigate a new self-supervised learning approach, called Mixing and Disentangling (MD), for point cloud pre-training. As the name implies, we explore how to separate the original point cloud from the mixed point cloud, and leverage this challenging task as a pretext optimization objective for model training. Considering the limited training data in the original dataset, which is much less than prevailing ImageNet, the mixing process can efficiently generate more high-quality samples. We build one baseline network to verify our intuition, which simply contains two modules, *i.e.*, encoder and decoder. Given a mixed point cloud, the encoder is first pre-trained to extract the semantic embedding. Then an instance-adaptive decoder is harnessed to disentangle the point clouds according to the embedding. Albeit simple, the encoder is inherently able to capture the point cloud keypoints after training and can be fast adapted to downstream tasks including classification and segmentation by the pre-training and fine-tuning paradigm. Extensive experiments on two datasets show that the encoder + ours (MD) significantly surpasses that of the encoder trained from scratch and converges quickly. In ablation studies, we further study the effect of each component and discuss the advantages of the proposed self-supervised learning strategy. We hope this self-supervised learning attempt on point clouds can pave the way for reducing the deeply-learned model dependence on large-scale labeled data and saving a lot of annotation costs in the future.

**Index Terms**—Self-supervised learning, Point cloud, Representation learning.

## I. INTRODUCTION

**P**POINT clouds, as the perception of the 3D world, have wide applications in many fields, such as autonomous driving [2]–[4] and virtual reality [5]. With the recent development of deep learning technology, deep learning-based approaches [6], [7] on point cloud processing gradually surpass traditional statistical processing methods [5], [8].

Inspired by the success in the image recognition task, the pre-training model on ImageNet can efficiently adapt to the new computer vision tasks, including image segmentation [9]–[12] and image retrieval [13]–[15]. The pre-training and fine-tuning paradigm has been widely adopted. However, the pre-training works on point cloud are still under-explored, and

Chao Sun is with School of Computer Science, Zhejiang University, Zhejiang, China. E-mail: c\_sun@zju.edu.cn

Zhedong Zheng and Yi Yang are with Centre for Artificial Intelligence, University of Technology Sydney, NSW, Australia. E-mail: zdzheng12@gmail.com, yi.yang@uts.edu.au

This work was partially sponsored by Zhejiang Lab’s International Talent Fund for Young Professionals (No.ZJ2020GZ021).

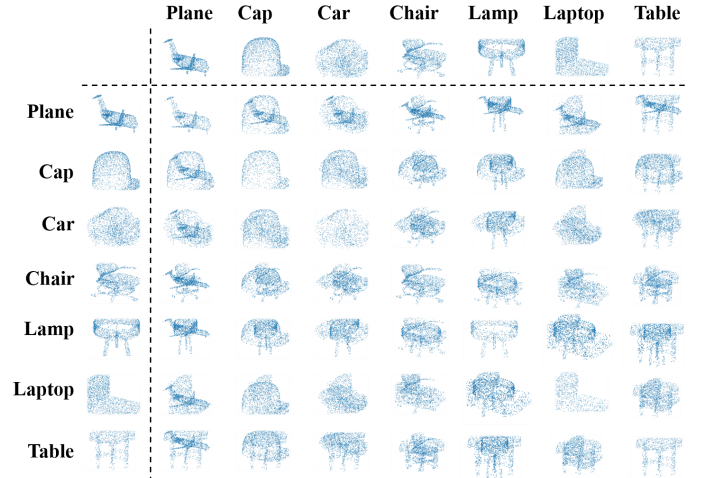


Fig. 1. Visualized results of mixed point clouds. We select seven types of point clouds from ShapeNet-Part [1]. Each row and column corresponds to original point clouds and the intersection corresponds to the mixed point cloud.  $M$  denotes the number of samples in the training set. **In theory, we can generate  $O(M \times M)$  different point clouds by sampling various cloud pairs, resulting in a much larger online generated training sample pool.**

limited work explores this direction. It is because that deeply-learned models are data-hungry. Although the point cloud data can be collected by laser sensors and other equipment, the point-wise point cloud annotation still costs a lot of human resources and unaffordable expenses [1], [16]–[18]. Therefore, in this work, we resort to self-supervised learning to reduce the demand for annotated data.

Most existing works [19], [20] focus on designing the pretext task by exploring the spatial characteristics of the single point cloud, which does not solve the problem of data limitation in current open-source datasets [1], [16]. In contrast, to address the data limitation, we design a potential solution to process two point clouds via mixing, without requiring any other steps, such as projection. Benefiting from the batch training of deeply-learned models, each point cloud can be mixed with a large number of point clouds during the whole training process. The proposed approach is memory and resource-efficient, which can directly process point clouds in a single pass. Compared with texture, which is important in 2D images, shape is a more important feature of the point cloud. We further propose a novel self-supervised task, Mixing and Disentangling (MD) in point clouds. The human can easily figure out the two 3D models, *i.e.*, chair and airplane, in the mixed point cloud, according to the prior knowledge on shape (see Figure 1). As the name implies, our intuition

underpinning the proposed **MD** is encouraging the neural network to learn similar knowledge, *i.e.*, shape-aware features, and such knowledge can be easily transferred to different classification and segmentation tasks. As shown in Figure 2, the pretext task of self-supervised learning is designed to separate the original point cloud from the mixed point cloud. In particular, the mixing means that the half points of two point clouds are mixed to obtain a new point cloud. The new point cloud contains the same number of points as the original point cloud. On the other hand, disentangling means separating the input point clouds from the mixed point cloud. The separating process demands the model to mine the key points of both two original point clouds from the mixed point cloud. This challenging task motivates the model to learn shape-related visual knowledge.

Briefly, our contributions are as follows:

- Comparing with most existing pre-training works on the image recognition, we do not have one million training 2D images as ImageNet [21]. To address this limitation in 3D point cloud, we leverage the mixing process to generate large-scale mixed data for model training;
- Inspired by the human ability to figure out two shapes from one mixed object, we propose a new self-supervised learning method on the point cloud, called Mixing and Disentangling (**MD**) to learn the geometric prior knowledge without the requisite of annotations;
- As one minor contribution, we implement one basic pipeline to verify the effectiveness of the proposed self-supervised learning strategy. It contains one encoder with the learnable aggregation function and one instance-adaptive decoder, to learn from the mixed point cloud and conduct the disentanglement.
- Albeit simple, experimental results on two benchmarks, *i.e.*, ModelNet-40 [16] and ShapeNet-Part [1], show that the self-supervised learning model can effectively and efficiently improve the accuracy of classification and segmentation tasks by the pre-training and fine-tuning paradigm. Self-supervised learning on the point cloud also can reduce the network dependence on labeled data. We hope this work could pave the way for future works in this field.

The rest of the paper is organized as follows. We first briefly introduce the relevant existing works in Section II, Section III describes the proposed method with detailed illustration and discussion on the pretext task. Experiments on both quantitative and qualitative performance verify the effectiveness of **MD** pre-training (see Section IV), followed by the conclusion in Section V.

## II. RELATED WORK

In this section, we focus our discussion on the relevant approaches investigating 3D point cloud processing and self-supervised learning.

### A. 3D Point Cloud Processing

In recent years, the approaches [22]–[25] based on deep learning plays an important role in the development of point

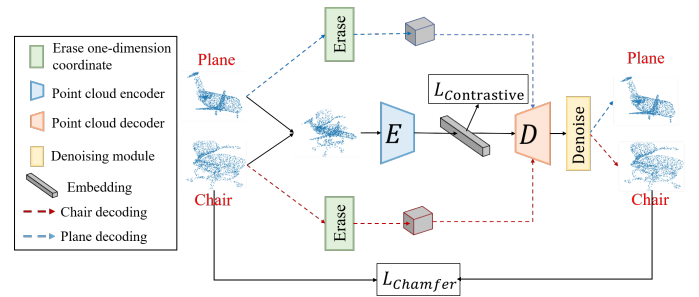


Fig. 2. A schematic overview of our method. The two original point clouds are mixed and input into encoder  $E$  to obtain the embedding vector of the mixed point cloud. A coordinate extracting operation,  $Erase$ , is used to extract partial information from the original point cloud for instance disentanglement. Then the embedding vector and instance information are input to the decoder  $D$  and the denoising module to generate the original point cloud, as shown in the red line and the blue line, respectively. The reconstruction loss, *i.e.*,  $L_{Chamfer}$ , between the generated point cloud and the original point cloud is used as the self-supervision during training.

cloud processing. Due to the irregular and disordered characteristics of point clouds, the traditional neural networks in the 2D field, *i.e.*, CNN, cannot be directly applied to point clouds. Therefore, the researchers resort to the other methods as follows to solve this problem.

**Voxel Based Method.** The voxel based method voxelizes the point cloud to obtain a cube with a grid structure, which can be directly processed by 3DCNN. The voxel based method [16], [26] can directly adopt the mature pipeline in 2D vision. However, the accuracy of this method is limited by the resolution during voxelization. High resolution can bring cubically increased memory usage, which will bring heavy computation costs when processing large-scale point clouds.

**Projection Based Method.** The projection based method [27]–[29] projects the point cloud on multiple planes. The existing 2D convolutional neural network is used to extract the projected point cloud features on different planes. After fusing multiple features, the feature descriptor of the point cloud is obtained, which can be used in downstream tasks. The projection-based method has achieved high accuracy in point cloud classification, but how to extend it to point-level tasks such as point cloud segmentation is still a difficult task.

**Point Based Method.** The previous work PointNet [30] proposed a neural network structure that directly processes the raw point cloud data. PointNet treats the point cloud as a point set, using a multi-layer perceptron (MLP) to process the original point cloud directly. A symmetric function is used to aggregate the features of all points, which meets the disorder of the point cloud. PointNet only considers the global feature, and PointNet++ [31] makes improvements to it, which considers both the global feature and the local feature. Point-based approaches can be divided into **graphed based method** and **convolution based method**. The graphed-based method treats the point set as a graph. This method aggregates the features of each point and the points in its neighborhood through the method of graph convolution. Pioneering works include DGCNN, etc [32], [33]. The convolution-based method introduces the concept of the convolution kernel in the 2D

convolution network into the point cloud. This type line of method defines multiple convolution kernels with different weights in space and obtains the feature description of the point cloud by summing the features of the points in the point cloud on each convolution kernel. The representative work of this method is KPConv [34], PAConv [35], etc. Taking one step further, various other methods also use explore attention and transformer. Point Transformer [36] uses the transformer structure for PointNet++, which improves the accuracy of classification and segmentation tasks. PCT [37] designed a point cloud processing network composed of transformers.

### B. Self-Supervised Learning

Self-supervised learning is a machine learning paradigm that uses the structural information of the data itself to generate labels required for training. This line of method pre-trains the model on the designed pretext task and then fine-tunes the above model on the downstream tasks to verify the effectiveness. (1). Some self-supervised learning methods based on the context of data. In particular, image rotations [38], image jigsaw puzzle [39], have been shown to be useful. (2). Some methods are based on the generation task. This type of methods learns the feature by image generation. Image coloring [40] is a method for coloring gray-scale images, which verifies the effect of self-supervised learning through the classification accuracy of gray-scale and color images. Super resolution method [41] apply adversarial learning to high-resolution reconstruction for a single image. Image inpainting [42] leverage the surrounding image information to infer the missing patch by context pixel prediction. Generative Adversarial Networks (GANs) is used for image generation [43], [44]. (3). Some self-supervised learning methods are based on contrastive learning. The type of methods leverages the structure information from data by designing loss functions. These methods define positive and negative samples firstly and then do representation learning can be completed by narrowing the distance between the same sample (positive pairs) and widening the distance between different samples (negative pairs). CPC [45] builds an end-to-end network and apply anti-noise estimation as the loss function. InfoNCE [45] propose a loss function based on mutual information for self-supervised learning. SimCIR [46] applies transformations such as scaling, flipping to obtain augmented samples and leverages these images to learn features. MoCo [47] compares contrastive learning to the process of looking up a dictionary and proposes the momentum updates mechanism. CoCLR [48] proposes the UberNCE loss, which adds the idea of semantic-class positives on the basis of infoNCE loss. Both MoCo and CoCLR prove that a large number of negative samples can improve the effect of model feature extraction. BYOL [49] solves the collapsing problem without using negative samples. Barlow Twins [50] does not use negatives pairs or momentum update. It focuses on making each dimension of the feature vector represent different information to improve the representation ability of features.

Similar to the situation of 2D image datasets, the annotation of 3D point clouds are usually unavailable due to the annotation time costs and human resource expense. In recent years,

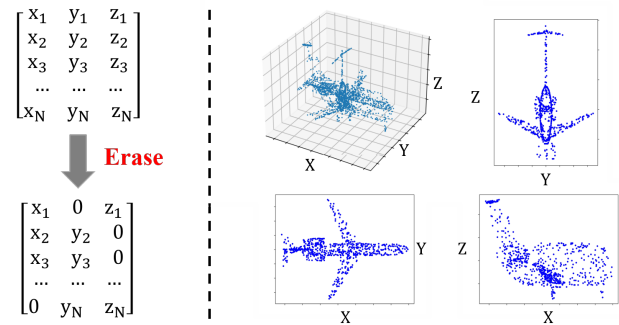


Fig. 3. The left part represents a point cloud of  $N$  points, and each point has 3D coordinates. After erasing, the random one-dimensional coordinate of each point in the input point cloud is set to zero which intends to make the pre-training process more challenging. The right part is the visualization of an erased point cloud of the plane and its three-view drawing after erasing. The erasing process equals randomly set about  $\frac{1}{3}N$  points to the corresponding projection surface.

there are several existing self-supervised learning methods, which also explore the point cloud pre-training. Inspired by the jigsaw problem in 2D space [39], Sauder *et al.* [19] propose a self-supervised learning algorithm based on space reconstruction. PointContrast [20] uses multi-view contrastive learning to match the shared points in two different views. They further pre-train the model on Scannet [18] and improve the accuracy of six downstream tasks includes classification, detection, etc. DepthContrast [51] proposes a self-supervised method based on contrastive learning which can handle different model architectures and different input data formats. The main difference between the proposed method and existing works are: 1). We generate more high-quality training point clouds via Mixing. This process largely increases the training pool and lets the model “see” more inlier variants during training. 2). The proposed pretext task is more challenging. Separating original objects from mixed point clouds is more difficult than extracting key points of a single object. 3). We also verify the effectiveness of the proposed method under the same setting, and show the learned model are competitive to downstream task as well.

## III. METHODOLOGY

In this section, we illustrate the baseline model, which simply contains two modules, *i.e.*, encoder and decoder. Then we explain the training strategy of Mixing and Disentangling. To further explain our intuition, we also provide the discussion to analyse the advantages of the corresponding components.

### A. Overview

As shown in Figure 2, the structure is mainly composed of one encoder and one decoder. The encoder is deployed to extract the embedding vector of the mixed point cloud. Given the output features of the encoder, the decoder is used to restore the original point clouds based on the embedding vector and partial coordinates of the original point cloud as the condition input. The embedding vector obtained from the encoder is sent to the decoder. Meanwhile, to separate the

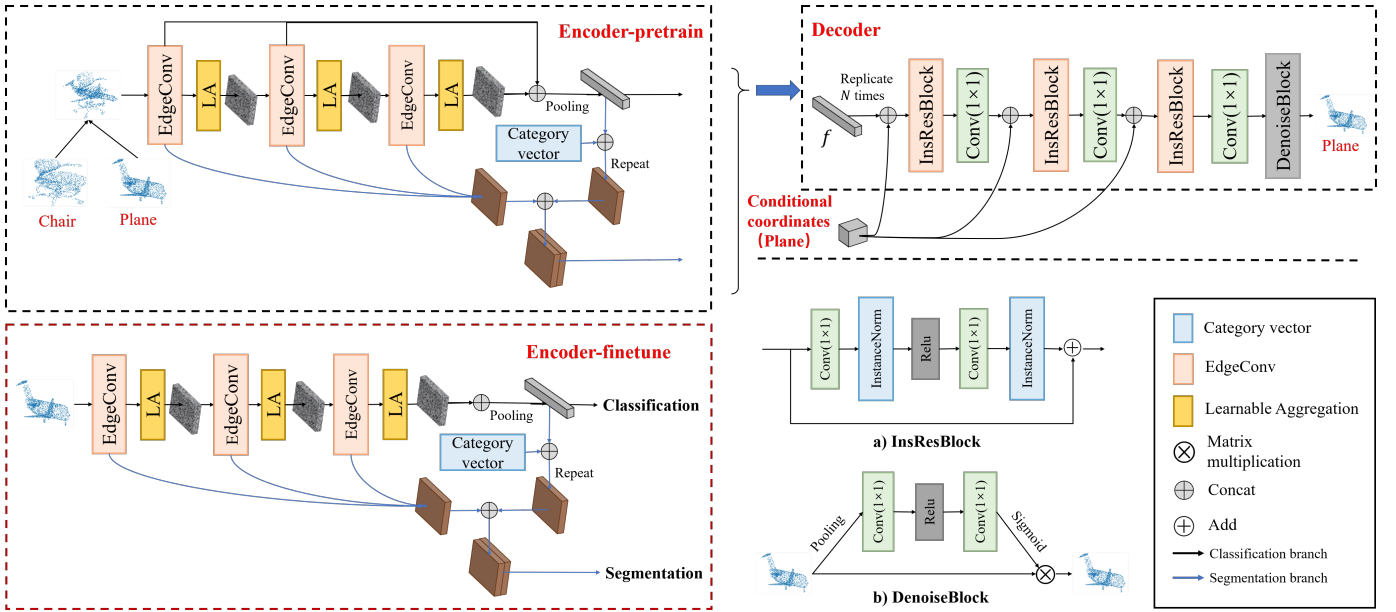


Fig. 4. **Model Structure.** The model is mainly composed of one encoder (left) and one decoder (right). **Encoder:** The encoder takes  $N$  points as input, and aggregates the special features of each point and its corresponding points in the neighborhood at an EdgeConv layer. The classification network (top branch) contains three EdgeConv layers and three learnable aggregation layers. The output of the encoder is the embedding vector  $f$  of the input point cloud. In the segmentation network, to concatenate with the point-wise feature from the shallow layers, the corresponding embedding vector  $f$  is repeated  $N$  times for point segmentation, where  $N$  is the number of points. The feature maps from shallow layers are concatenated with the embedding vector to obtain the multiple-scale feature map as the output of the encoder. Different from the classification branch, the category vector representing the type of point cloud is fused into the embedding vector for the part segmentation. **Decoder:** The decoder is composed of Instance-aware Residual Block (InsResBlock),  $1 \times 1$  Convolutional Layers and one DenoiseBlock to refine the final reconstructed point cloud. The structure of the residual module and denoising module is shown in a) and b). The random two-dimensional coordinates of the original point cloud are used as conditional information to be fused with the backbone features in three different layers.

original point cloud from the mixed point cloud, we apply the random two-dimensional coordinates of the original point cloud as additional information into the decoder after erasing (see Figure 3). The output of the decoder is the original point cloud recovered from the embedding vector. After pre-training the model, the encoder can be utilized to extract decent features for sub-sequential tasks. If the task is the point cloud classification, the black arrows are used as the recognition workflow. Otherwise, the segmentation task demands extra low-level information and the point cloud category. It is because different objects contain different semantic parts. For instance, the plane contains aircraft nose, plane body, plane tail and wings while the chair has legs, the seat and the back. For the point part segmentation, we add the category vector and concatenate the activations from the shallow network. As shown in Figure 4, blue arrows denote the extra workflow for the segmentation task. In the following subsection, we first illustrate the encoder structure to learn the geometric representation from the mixed point cloud.

### B. Encoder

Given a point cloud, the encoder is used to extract the embedding vector. We denote the point cloud as a set of points  $S = \{s_1, s_2, \dots, s_n\}$ ,  $x_i \in \mathbb{R}^3$  and each point has 3D coordinates. The encoder converts it into an embedding vector  $f$ . However, the point cloud does not have a regular spatial structure as 2D images, we can not apply the convolutional neural network (CNN) directly. Therefore, we deploy the graph

convolutional network (GCN) to overcome this limitation. Similar to convolution in CNN, we leverage the GCN to gather neighbor points around a certain point to acquire local information. In particular, we apply the graph convolution to aggregate the features of neighbor points to the center point and update the feature of the center point. Specifically, we harness the graph  $\mathcal{G}$  to represent the relationship among each point. The relationship can be expressed as  $\mathcal{G} = (\mathcal{V}, \mathcal{E})$ , where  $\mathcal{V}$  represents the set of vertices and  $\mathcal{E} \subseteq \mathcal{V} \times \mathcal{V}$  represents the edge set. We apply K-Nearest Neighbor (KNN) algorithm to construct the graph  $\mathcal{G}$  in the feature space. The KNN algorithm based on the feature inputs can efficiently and effectively find two points with the most similar semantics, *i.e.*, the points on the two legs of the chair, which have similar semantics. It makes the model easy to capture the key parts in the input point cloud. We further deploy EdgeConv layers to leverage the graph information. Given the input of  $N \times C_{in}$  and the corresponding graph  $\mathcal{G}$ , the EdgeConv layer performs feature transformation on the  $N$  points and output the updated point features of  $N \times C_{out}$ . The input features can be represented as  $X = \{x_1, x_2, \dots, x_n\}$ ,  $x_i \in \mathbb{R}^{C_{in}}$  where  $x_i$  represents the feature of point  $i$ . The relation feature  $r_i^k \in \mathbb{R}^{N \times C_{out}}$ , which can be formulated as:

$$r_i^k = MLP(\text{concat}(x_i, x_i - x_k)), k : (i, k) \in \mathcal{E}, k \neq i, \quad (1)$$

explicitly encodes the relationship between  $x_i$  and  $x_k$ , where  $x_k$  is the  $k$ -th neighbor of  $x_i$  and  $MLP$  notes a linear function with ReLU [52]. To update the point feature  $x_i$ , we apply

Learnable Aggregation (LA) as the aggregation method to the local structure  $r_i^k$  of the neighbors.

$$LA(x_i) = \alpha \times \max_{(i,k) \in \mathcal{E}, k \neq i} (r_i^k) + (1-\alpha) \times \text{avg}_{(i,k) \in \mathcal{E}, k \neq i} (r_i^k). \quad (2)$$

We notice that the current widely-used aggregation methods applied in the point cloud include both max pooling and average pooling. It is usually challenging to decide which pooling function should be used. As one minor contribution, we involve one learnable pooling layer in the model and let the model end-to-end learn the adaptive weight by itself. As shown in Eq. 2, LA is a linear interpolation of max pooling and average pooling, where the interpolation ratio  $\alpha$  is a learnable parameter of the network. If  $\alpha = 0$ , LA is equivalent to average pooling and if  $\alpha = 1$ , it is equivalent to max pooling. We have verified the effectiveness of LA through extensive experiments and more results are provided in the Experiment. The result also shows the aggregation function in shallow layers prefers the average of both mean and max pooling, while the aggregation function in deep layers prefers to capture the salient region and tends to choose the max pooling.

As shown in Figure 4, the encoder for pre-training has two branches: classification and segmentation. The backbone of the encoder is composed of three EdgeConv layers and three LA layers. We use skip connections to add the low-level information from shallow networks. The output features of the last EdgeConv layer are aggregated globally to form a one-dimensional embedding. For the classification task, the embedding is used as the feature vector of the mixed point cloud which is sent to the decoder. As for the segmentation, which is a point level task, we add the extra category vector and concatenate the features from the shallow network to keep the same structure for fine-tuning.

**Discussion.** By using the proposed mixing mechanism, we can generate more high quality point cloud samples, which largely enriches training samples. The previous methods [19] uses ShapeNet-Part for pre-training and it can only generate  $O(M)$  training samples, where  $M$  is the number of point clouds. In theory, our method can generate  $O(M \times M)$  different point clouds by sampling various cloud pairs, resulting in a much larger online generated training sample pool. The encoder can extract more prior knowledge from data, which improves downstream tasks. Besides, to extract the features more efficiently, we propose a new feature aggregation method LA in the point cloud. Most existing works [31], [33] apply max pooling to aggregate the neighboring features, which lead to much information loss. LA leverages a learnable parameter to dynamically adjust the aggregation method, which can effectively retain the local structure. More ablation studies on LA is provided in the experiment.

### C. Decoder

We propose an instance-adaptive decoder, which can restore the input point cloud from the embedding vector according to the conditional coordinates adaptively. The decoder treats the embedding vector as structure representation of the mixed point cloud and aims to disentangle key points from different

objects. In our network, the decoder is utilized as a selective filter, which gradually enhances the feature of points belonging to one object and weakens the feature of the rest points of another object. After several transformations, the feature mainly contains the key points of one object, which can be transformed to the recovered point cloud by the final linear layers. As shown in Figure 4, the decoder is composed of Instance-aware Residual Block (InsResBlock),  $1 \times 1$  Convolution Layers and one denoising module *i.e.*, Denoise Block. There are two inputs to the decoder: the mixed point cloud embedding vector  $f$ , the conditional coordinates  $C_{coord}$  of size  $N \times 3$ .

To recover the original point cloud from the mixed feature, extra information  $C_{coord}$  of each of the two point clouds is given. We use the random two-dimensional coordinates of the original point cloud as partial information. As shown in Figure 3, we randomly erase one of the three coordinates of each point cloud. For each point in a point cloud, the erased dimensions are randomly generated instead of taking a certain dimension. Since the direct erasing of a certain dimension will cause the point cloud to change from  $N \times 3$  to  $N \times 2$ , and the neural network cannot distinguish the specific dimensions of the remaining two coordinates. For instance, the model can not foreknow the two coordinates are (X,Y) or (X,Z) or (Y,Z). We choose to set the erasing coordinates to zero instead of directly deleting the dimension.

Instance-aware Residual Block (InsResBlock) is a basic module used to disentangle the mixed feature from  $f$  according to the conditional coordinates  $C_{coord}$ . The structure of InsResBlock is shown in Figure 4 (a), which is composed of two convolution layers. Skip connection is used to concatenate the information from the input. The  $1 \times 1$  convolution layer is applied to reduce the feature dimension. A pair of InsResBlock and  $1 \times 1$  convolution layer is regarded as a basic decoding unit. Our decoder  $D$  is built with three sequential basic decoding units. Three decoding units connected sequentially reduce the feature dimension layer by layer and finally output the generated point cloud of 3 coordinate channels. For each basic encoding unit, to strengthen the conditional coordinates, we concatenate the conditional coordinates and the feature from the previous unit and send the combined structure representation to the next unit.

The point cloud generated by above parts inevitably contains noise, so a denoising module is introduced. As shown in Figure 4 (b), the denoising module is implemented via a self-attention manner. The module leverages the context information between neighbor points to assign different weights for adjacent points and noisy points, which can ensure each point will be optimized with the global information. Given the noisy point cloud  $\tilde{s}$ , the denoising module outputs the denoising point cloud  $\hat{s} = \text{Denoise}(\tilde{s})$ ,  $\tilde{s} = D(f, C_{coord})$ , where  $D$  represents the decoder. In particular, given the tensor  $\tilde{s}$  of  $N \times 3$ , we perform average pooling in the dimension of  $N$  to obtain an initial weight of  $N \times 1$  for every point. After two convolution layers, which can be viewed as fully connected layers to aggregate the global information from all points, the global information for every point is provided into the sigmoid function to obtain the normalized weight of each key

point. Then the weight is multiplied by the original point cloud to obtain the denoised point cloud. The multiplication allows every point to refer to the neighbor points and ignore outlier points with low scores, according to the point-wise weights.

**Discussion. The choice of conditional disentanglement.** The choice of  $C_{coord}$  has a huge impact on the reconstruction results and downstream tasks. If the decoder can only obtain little original point cloud information from  $C_{coord}$ , the reconstruction effect of disentanglement will be poor. On the contrary, if the decoder obtains too much information of the original point cloud, the decoder will restore the original point cloud based on the conditional information directly. Then the encoder cannot be well trained to fully mine the geometric information. We think this choice is still open and in this paper, we observe that using random two-dimensional coordinates is a balanced choice, which guarantees the completeness of the disentanglement and the challenge of the pre-training task.

#### D. Optimization

The loss function of the network is composed of two parts, including the embedding loss and the point cloud reconstruction loss. As the main parts of the proposed Mixing and Disentangling task (MD), we supervise the model training by the disentanglement results via the reconstruction. In practise, mixing two point clouds is to randomly sample half points of two input point clouds as one mixed point cloud. Disentangling means to recover the two original input clouds from the mixed point cloud. Besides, we add the intermediate embedding loss for self-supervision. There are many different candidates for the embedding loss. In this work, without loss of the generality, we select the contrastive learning to verify the compatibility of the proposed method to different losses instead of pursuing the best performance. Next, we will describe the two optimizing objectives with details.

**Reconstruction loss.** Reconstructed point clouds can be obtained from the embedding vector  $f$  and the conditional coordinates  $C_{coord}$ . The decoding process can be noted by  $\hat{s} = D(f, C_{coord})$ , where  $D$  represents the decoder. We apply Chamfer distance to measure the distance between two point clouds. As Eq. 3 shows, the distance is a symmetric function. Since we could not know the exact matching between two point sets, the Chamfer distance accumulates one sub-optimal but effective distance between the closest points in both the source and target point cloud.  $\|\cdot\|_2$  denotes the L2 distance between two points. The reconstruction loss can be formulated as:

$$L_{Chamfer} = \frac{1}{|\hat{s}|} \sum_{\hat{p} \in \hat{s}} \min_{p \in s} \|p - \hat{p}\|_2 + \frac{1}{|s|} \sum_{p \in s} \min_{\hat{p} \in \hat{s}} \|\hat{p} - p\|_2, \quad (3)$$

where  $s$  represents the original point clouds before mixing and  $p$  denotes the point position in  $s$ .  $\hat{s}$  denotes the reconstructed point clouds, and  $\hat{p}$  denote the points in  $\hat{s}$ . Specifically, we apply the chamfer distance as the reconstruction loss on  $s$  and  $\hat{s}$ . In practise, since we mix two input point clouds, we will calculate two Chamfer losses for the two reconstructed point clouds and accumulate the losses.

**Embedding loss.** Inspired by the contrastive loss [53], we introduce it to our total loss function, which intends to widen object pairs of different categories. In particular, ShapeNet-Part has a total of 16 categories of objects, and we can generate  $16 \times 16 = 256$  categories of different mixed point clouds. Under the pre-training setting, we do not know the actual labels of the generated samples, so we follow the existing practise, e.g., Instance loss [54] and MoCo [47], to view every sample as one single category. We encourage that these point clouds should have different embedding and we deploy this as an optimization objective. During training, each batch contains  $B$  different mixed point clouds. Ideally, each mixed point cloud has low similarity with other point clouds and has high similarity with itself. We note the input mixed point clouds as  $s_i$ , and embedding vector  $f_i$  can be obtained by  $f_i = E(s_i)$ , where  $E$  notes the encoder. Then we can construct  $B \times B$  pairs of samples by matching calculating the similarity between every pair among the batch. The basic contrastive loss can be formulated as:

$$L_{Contrastive} = \frac{1}{B^2} \sum_{i=1}^B \sum_{j=1}^B \left[ yG(i, j)^2 + (1 - y) \max(0, 1 - G(i, j))^2 \right]. \quad (4)$$

where  $y = 1$  when two samples are the same  $i == j$ , otherwise  $y = 0$ .  $G(i, j)$  is used to note the distance between sample  $i$  and sample  $j$  in the feature space. For simplicity, we apply cosine similarity to metric the distance of two embedding vectors. We set  $G(i, j) = 1 - \text{cosine}(f_i, f_j)$ , where  $\text{cosine}$  notes cosine similarity. The above loss function can be simplified as:

$$L_{Contrastive} = \frac{1}{B^2} \sum_{i=1}^B \sum_{j=1}^B \left[ y(1 - \text{cosine}(f_i, f_j))^2 + (1 - y) \max(0, \text{cosine}(f_i, f_j))^2 \right]. \quad (5)$$

Given the embedding vector  $f_i$  and  $f_j$ , the cosine similarity matrix is obtained by  $Q_{ij} = \frac{f_i}{\|f_i\|} \times \frac{f_j}{\|f_j\|}$ . When  $i = j$ ,  $Q_{ij} = 1$ . Otherwise,  $Q_{ij} \in [-1, 1]$ . We can further make the Eq. 5 to the matrix format for better efficiency as well as the global distance optimization. Eq. 5 contains  $B \times B$  elements, which is corresponding to  $B \times B$  positions of the  $Q$ . We linearly rescale the similarity matrix  $Q$  to  $[0, 1]$  and intends to optimize the distance between  $\frac{Q+1}{2}$  and an identity matrix  $I_{B \times B}$ . In the implementation, we use L1 loss instead of L2 loss, so we can simply apply an L1 loss between  $\frac{Q+1}{2}$  and the identity matrix  $I$  to build our loss function, which is:

$$L_{Contrastive} = \left| \frac{Q+1}{2} - I \right|. \quad (6)$$

Therefore, to optimize the parameters in both encoder and decoder, we deploy the total loss as follows:

$$L_{total} = L_{Chamfer} + \lambda L_{Contrastive}. \quad (7)$$

where  $\lambda$  is the weight to control the Contrastive loss. Actually, Contrastive loss is an optional choice. In the ablation studies, we also study the effect of Contrastive loss by setting  $\lambda = 0$ . More details can be found in the following section.

## IV. EXPERIMENT

### A. Datasets

**ModelNet-40** [16] is sampled from the mesh surfaces of CAD models, containing 40 categories, 12,311 models. 9,843 models are used for training and 2468 are reserved for testing. Each point cloud contains 2048 points and the coordinates of all points are normalized into the unit sphere. Follow the experimental setting of most existing works [33], [57], we sample 1024 points from each object and augment the data by randomly scaling objects and perturbing point locations.

**ShapeNet-Part** [58] is sampled on the CAD models, having a total of 16,881 point clouds, of which 12,137 point clouds are used for training, 1870 point clouds are used for verifying, and 2874 point clouds are used for testing. Each point cloud is composed of 2048 points, and the coordinates of all points are normalized into the unit sphere. We sample 1024 points from each object. Each point has four attributes including the 3D coordinates of each point, the category label of the model, and the category label of each point.

### B. Implementation Details

The pre-trained model is trained with Adam optimizer ( $\beta_1 = 0.9, \beta_2 = 0.99$ ) of a minibatch of 12. The initial learning rate is set to 0.1. We gradually decrease the learning rate via the cosine policy [59], and the model is trained for 100 epochs. We use position jittering as a data augmentation method, which directly adds Gaussian noise to every coordinate of input point clouds. Following the experimental setting of most existing works [33], [57], we set  $k = 20$  for KNN algorithm and use the dynamic graph instead of the fixed graph. In the classification network, there are four EdgeConv layers and the channel number is  $\{64, 64, 128, 256\}$ . In the segmentation network, there are three EdgeConv layers and the channel number is  $\{64, 64, 64\}$ . Two dropouts with 0.5 drop probability are used when fusing the conditional coordinates and the embedding vector. The pre-train model is trained from scratch on 3D point clouds and the training time is about one day.

In the fine-tuning stage, we apply the same settings to train the model from scratch and the pre-trained model. We set  $k = 20$  for KNN algorithm and sample 1024 points in each point cloud. The classifiers for classification and segmentation are added to the encoder. For classification and segmentation networks, we train 250 and 100 epochs respectively.

In the segmentation network, there is a different setting between the pre-training and fine-tuning stages. As shown in Figure 4 encoder part, the segmentation task demands the category of the point cloud. In the pre-training stage a random category of the two original point cloud classes is given to each object and in the fine-tuning stage we give the real category vector of each object.

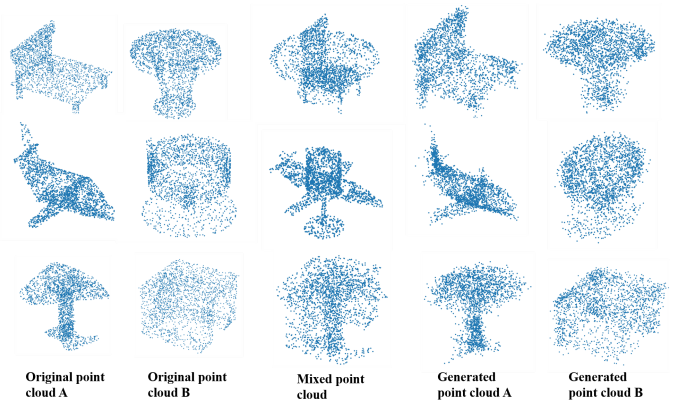


Fig. 5. Visualization of recovered point clouds after disentanglement. The experiment is performed on the ShapeNet-Part. Two columns on the left are the original point clouds and the middle column shows mixed point clouds. Two columns on the right are the corresponding generated point clouds recovered from the mixed point cloud. We observe that the proposed method can successfully disentangle the mixed point cloud to two separate point clouds.

### C. Quantitative Results

**Baseline for training from scratch.** We adopt the model shown in Figure 4 fine-tuning part and use the training and testing procedure described in Implementation Details. As shown in Table I, we report the accuracy of three widely-used backbones in the point cloud and our model without pre-training, which is treated as the baseline. The result shows our baseline model achieves an overall accuracy of 92.74% and mean class accuracy of 89.88% in the classification task and 85.27% mean IoU (%) in the segmentation task.

**The pre-training improves the baseline.** We evaluate how the pre-training affect the performance. Results are shown in Table I. For the classification task, the model is pre-trained and finetuned on ModelNet-40. We note that the pre-trained model gets the overall accuracy of 92.87%, which have +0.65% improvements to baseline. Similarly, the mean class accuracy also increases from 89.88% to 90.26% with +0.38% accuracy improvement. For the segmentation task, the model is pre-trained and finetuned on ShapeNet-Part. The pre-trained model achieves the rank-1 mean Intersection-over-Union (mIoU) of 85.50%. Experimental results show that the accuracy of our baseline surpasses three existing works in the table, and pre-training can still bring gains to the accuracy on this basis. Overall, pre-training can bring improvements both in classification and segmentation tasks, which verifies the effectiveness of our pretext task.

### D. Qualitative Results

**Visualization of the reconstructed point cloud after disentanglement.** As shown in Figure 5, we visualize original point clouds, mixed point clouds, and generated point clouds on ShapeNet-Part. We visualize three sets of point clouds. Each row in the figure is the original point cloud A, the original point cloud B, the mixed point cloud, and two generated point clouds correspondingly. Overall, our method achieves ideal visualization results.

TABLE I

RESULTS FOR OUR BASELINE AND BASELINE + PRE-TRAINING. WE CARRY OUT TWO EXPERIMENTS OF CLASSIFICATION AND SEGMENTATION, WHICH ARE PERFORMED ON MODELNET-40 AND SHAPENET-PART RESPECTIVELY. WE FURTHER COMPARE THREE COMPETITIVE APPROACHES IN THE POINT CLOUD. ALL MODELS ARE TRAINED WITH 1024 POINTS. THE BASELINE MODEL WITH PRE-TRAINING ACHIEVES THE HIGHEST ACCURACY IN THE TABLE.

Methods	ModelNet-40 ( <i>Classification</i> )		ShapeNet-Part ( <i>Segmentation</i> )
	Overall Accuracy (%)	Mean Class Accuracy (%)	mean IoU (%)
3DShapeNets [16]	84.7	77.3	-
VoxNet [26]	85.9	83.0	-
PointNet [30]	89.2	86.0	83.7
SpecGCN [55]	91.5	-	-
PointNet++ [31]	91.9	-	85.1
PCNN by Ext [56]	92.2	-	85.1
DGCNN [33]	92.9	90.2	85.1
Ours (from scratch)	92.74	89.88	85.27
Ours (pre-training)	<b>93.39</b>	<b>90.26</b>	<b>85.50</b>

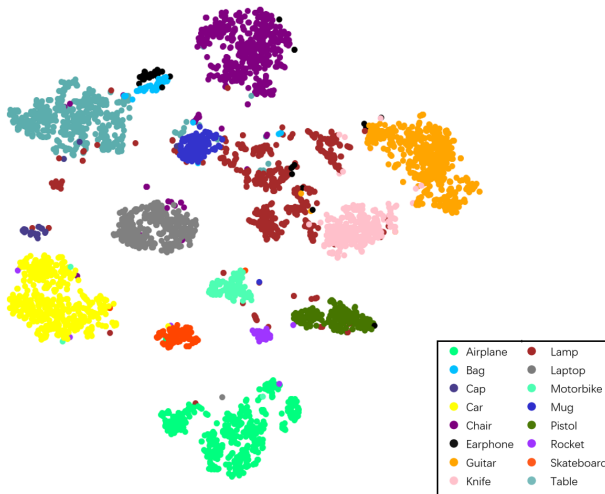


Fig. 6. The visualization of embedding vector of ShapeNet-Part in the semantic space via T-SNE [60]. The encoder is pre-trained on ModelNet-40 and is applied to encode the point clouds on ShapeNet-Part directly. The results show that the distance between intra-class samples is small while the distance between inter-class data is large, which verifies that our encoder learns a robust and general structure embedding vector. The Mixing and disentangling pre-training provides one good initial representation, even when the model has not seen any point clouds from the segmentation dataset, *i.e.*, ShapeNet-Part.

**Visualization of Embedding.** We visualize the embedding vector obtained by the encoder. The encoder is pre-trained on ModelNet-40 and we obtain the embedding vectors of ShapeNet-Part with the pre-trained encoder. We apply the T-SNE [60] to reduce the dimension of the embedding vector to  $\mathbb{R}^2$ . As shown in Figure 6, most categories are separated easily. The distance between intra-class samples is small and the distance between inter-class is large. The above result proves the generalization of the encoder to unseen point clouds from the segmentation dataset, *i.e.*, ShapeNet-Part.

TABLE II

SEGMENTATION RESULTS ON RARE LABELED DATA. WE COMPARE THE ACCURACY BETWEEN THE MODEL TRAINED FROM SCRATCH AND THE PRE-TRAINED MODEL UNDER DIFFERENT LABELED DATA RATIOS. THE PERFORMANCE BOOST IS MORE SIGNIFICANT WHEN THE ANNOTATED TRAINING DATA IS LIMITED. THE OBSERVATION IS ALIGNED WITH OUR INTUITION TO BENEFIT THE REAL-WORLD MODEL TRAINING PROCESS UNDER THE DATA LIMITATION.

Labeled Data Ratio (%)	Pre-trained	Average Accuracy (%)	mean IoU (%)
10		74.02	81.59
10	✓	77.04	82.23
25		80.39	83.76
25	✓	81.11	84.49
50		81.46	84.71
50	✓	83.31	85.04

### E. Ablation Studies and Further Discussion

**What Happens when Labeled Data is Limited?** In real scenes, we often cannot get enough labeled data. To simulate this situation, we divide the original dataset into two parts  $A$  and  $B$ , and regard  $A$  as unlabeled data. In self-supervised learning, we use  $A + B$  to pre-train the model. When training downstream tasks, we only use  $B$ . We set the percentages of labeled data as 10%, 25%, and 50% respectively. The experiment is set a segmentation task and performed on ShapeNet Part. We verify the effect of self-supervised learning by comparing the accuracy of the encoder trained from scratch with the accuracy of the pre-trained encoder. We report the results in Table II. The results show that as the amount of labeled data decreases, the accuracy of segmentation gradually decreases when the labeled data is reduced. But the accuracy of the pre-trained model surpasses that of the model trained from scratch significantly. This shows that our method can leverage unlabeled data to improve the accuracy of the model when the amount of labeled data is insufficient.

**Ablation study on LA and Contrastive Loss.** We use LA to aggregate neighbor point features. To verify the effect of LA, we use the same network architecture to test the accuracy of LA and max pooling. As shown in Table IV, regardless of pre-training, the accuracy of using LA is higher than that of using max pooling, which verifies that LA can better preserve

TABLE III

RESULTS OF USING POINTNET++ [31] AS THE BACKBONE. TO VERIFY THE VERSATILITY OF OUR METHOD, WE USE POINTNET++ AS THE BACKBONE AND COMPARE THE ACCURACY BETWEEN THE MODEL TRAINED FROM SCRATCH AND THE PRE-TRAINED MODEL. WE OBTAIN ONE CONSISTENT RESULT THAT OUR METHOD IS COMPATIBLE WITH DIFFERENT NETWORK STRUCTURES AND CAN STILL IMPROVE THE ACCURACY OF CLASSIFICATION AND SEGMENTATION TASKS EVEN WHEN THE BACKBONE IS CHANGED. \*: WE RE-IMPLEMENT THE MODEL, WHICH ACHIEVES ONE SLIGHTLY BETTER PERFORMANCE.

Methods	ModelNet-40 ( <i>Classification</i> )		ShapeNet-Part ( <i>Segmentation</i> )
	Overall Accuracy (%)	Mean Class Accuracy (%)	mean IoU (%)
PointNet++ (from scratch)	91.9	-	85.1
PointNet++* (from scratch)	92.07	88.89	85.20
PointNet++* (pre-training)	<b>92.57</b>	<b>89.96</b>	<b>85.27</b>

TABLE IV

ABLATION STUDY ON DIFFERENT COMPONENTS DURING THE MODEL TRAINING. WE VERIFY THE EFFECTS OF THE LA MODULE AND CONTRASTIVE LOSS. WE USE THE SAME NETWORK ARCHITECTURE FOR EXPERIMENTS, EXCEPT FOR THE AGGREGATE FUNCTION. IN THE CONDITION OF APPLYING LA, WE FURTHER EXPLORE THE EFFECT OF CONTRASTIVE LOSS, WHICH IS SHOWN IN THE LAST THREE ROWS IN THE TABLE.

Pooling Method	Pre-trained	Contrastive loss	mean IOU (%)
Max Pooling			85.17
Max Pooling	✓		85.34
LA			85.27
LA	✓		85.40
LA	✓	✓	85.50

the local structure of the point cloud.

We apply Contrastive loss to narrow the distance between similar samples and widen the distance between different samples. The encoder can extract more robust embedding from data, which can improve downstream tasks. We use the segmentation task on Shapenet-Part to confirm our method. We train two pre-trained models with or without Contrastive loss and then fine-tune the two models in the same experimental settings, and finally compare the segmentation accuracy of the two models. Results are shown in Table IV. We note that both pre-training and Contrastive loss can improve the segmentation task, which verifies our idea.

**Ablation study on Denoising Block.** The visualization results are shown in Figure 7. a) is the original point cloud, and b) is the generated point cloud obtained by the network without the denoising module. c) is the generated point cloud obtained by the network with the denoising module. We can find that there is a noise point circled in the red circle of b) and there is no such point in c). The denoising module pulls the noise point back to the center of the point cloud, which verifies the effect of the denoising module.

**Effectiveness with different backbone structures.** To verify that our pretext task is free from the choice of backbones, we further explore leveraging the widely-adopted network as the backbone of the point cloud encoder. PointNet++ [31] is a widely-used point cloud processing network, which is usually used in classification and segmentation. We apply the encoder of PointNet++ to replace that of our encoder backbone. Then we compare the accuracy of the model trained from scratch

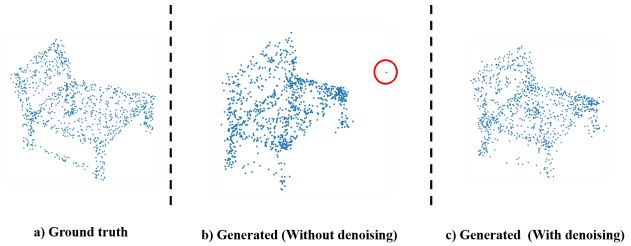


Fig. 7. Visualization results of generated point clouds. The original point cloud is shown in a). b) is the generated point cloud without denoising and c) is the point cloud after denoising. The result shows that the denoise module can help to remove the noise point circled in b).

and the pre-trained model. We carry out two experiments of classification and segmentation respectively and results are shown in Table III. The results show the accuracy of the pre-trained model surpasses the baseline, which verifies the versatility of our proposed method.

## V. CONCLUSION

In this paper, we propose a new self-supervised learning method, called Mixing and Disentangling (MD), for point cloud pre-training. Different from the existing works, we propose to mix the original point clouds in the training set to form “new” data and then demand the model to “separate” the mixed point cloud. In this way, the model is asked to mine the geometric knowledge, such as the shape-related key points for reconstruction. To verify the effectiveness of the proposed method, we build a simple baseline to implement our method. We use an encoder to obtain the embedding of the mixed point cloud and then an instance-adaptive decoder is harnessed to separate the original point clouds. During the self-supervised training, the encoder learns the prior knowledge of point cloud structure, which is scalable and can improve the downstream tasks. Experiments show consistent performance improvement through classification and segmentation tasks and verify the effectiveness of our method especially when the number of labeled data is limited. We hope that our approach can benefit the future point cloud works, and take one closer step to the harsh real-world setting, *i.e.*, limited annotations. In the future, we will continue to study the point cloud pre-training method on large-scale datasets, and focus on finding an efficient way to take advantage of the large-scale point data.

## REFERENCES

- [1] L. Yi, V. G. Kim, D. Ceylan, I.-C. Shen, M. Yan, H. Su, C. Lu, Q. Huang, A. Sheffer, and L. Guibas, "A scalable active framework for region annotation in 3d shape collections," *ACM Transactions on Graphics (ToG)*, vol. 35, no. 6, pp. 1–12, 2016.
- [2] Y. Cui, R. Chen, W. Chu, L. Chen, D. Tian, Y. Li, and D. Cao, "Deep learning for image and point cloud fusion in autonomous driving: A review," *IEEE Transactions on Intelligent Transportation Systems*, 2021.
- [3] Y. Li, L. Ma, Z. Zhong, F. Liu, M. A. Chapman, D. Cao, and J. Li, "Deep learning for lidar point clouds in autonomous driving: a review," *IEEE Transactions on Neural Networks and Learning Systems*, 2020.
- [4] A. Tampuu, T. Matiisen, M. Semikin, D. Fishman, and N. Muhammad, "A survey of end-to-end driving: Architectures and training methods," *IEEE Transactions on Neural Networks and Learning Systems*, 2020.
- [5] Y. Guo, H. Wang, Q. Hu, H. Liu, L. Liu, and M. Bennamoun, "Deep learning for 3d point clouds: A survey," *IEEE transactions on pattern analysis and machine intelligence*, 2020.
- [6] T. Wan, S. Du, W. Cui, R. Yao, Y. Ge, C. Li, Y. Gao, and N. Zheng, "Rgb-d point cloud registration based on salient object detection," *IEEE transactions on neural networks and learning systems*, 2021.
- [7] Y. Chen, H. Li, R. Gao, and D. Zhao, "Boost 3-d object detection via point clouds segmentation and fused 3-d giou-l loss," *IEEE Transactions on Neural Networks and Learning Systems*, 2020.
- [8] X. Huang, G. Mei, J. Zhang, and R. Abbas, "A comprehensive survey on point cloud registration," *arXiv preprint arXiv:2103.02690*, 2021.
- [9] O. Ronneberger, P. Fischer, and T. Brox, "U-net: Convolutional networks for biomedical image segmentation," *Springer International Publishing*, 2015.
- [10] J. Long, E. Shelhamer, and T. Darrell, "Fully convolutional networks for semantic segmentation," in *Proceedings of the IEEE conference on computer vision and pattern recognition*, 2015, pp. 3431–3440.
- [11] H. Zhao, J. Shi, X. Qi, X. Wang, and J. Jia, "Pyramid scene parsing network," *IEEE Computer Society*, 2016.
- [12] L. C. Chen, Y. Zhu, G. Papandreou, F. Schroff, and H. Adam, "Encoder-decoder with atrous separable convolution for semantic image segmentation," in *European Conference on Computer Vision*, 2018.
- [13] A. Gordo, J. Almazán, J. Revaud, and D. Larlus, "Deep image retrieval: Learning global representations for image search," in *European Conference on Computer Vision*, 2016.
- [14] H. Yao, S. Zhang, D. Zhang, Y. Zhang, and T. Qi, "Large-scale person re-identification as retrieval," in *2017 IEEE International Conference on Multimedia and Expo (ICME)*, 2017.
- [15] Z. Zheng, Z. Liang, and Y. Yi, "Unlabeled samples generated by gan improve the person re-identification baseline in vitro," in *IEEE International Conference on Computer Vision*, 2017.
- [16] Z. Wu, S. Song, A. Khosla, F. Yu, L. Zhang, X. Tang, and J. Xiao, "3d shapenets: A deep representation for volumetric shapes," in *Proceedings of the IEEE conference on computer vision and pattern recognition*, 2015, pp. 1912–1920.
- [17] I. Armeni, S. Sax, A. R. Zamir, and S. Savarese, "Joint 2d-3d-semantic data for indoor scene understanding," *arXiv preprint arXiv:1702.01105*, 2017.
- [18] A. Dai, A. X. Chang, M. Savva, M. Halber, T. Funkhouser, and M. Nießner, "Scannet: Richly-annotated 3d reconstructions of indoor scenes," in *Proceedings of the IEEE conference on computer vision and pattern recognition*, 2017, pp. 5828–5839.
- [19] J. Sauder and B. Sievers, "Self-supervised deep learning on point clouds by reconstructing space," *arXiv preprint arXiv:1901.08396*, 2019.
- [20] S. Xie, J. Gu, D. Guo, C. R. Qi, L. Guibas, and O. Litany, "Pointcontrast: Unsupervised pre-training for 3d point cloud understanding," in *European Conference on Computer Vision*. Springer, 2020, pp. 574–591.
- [21] O. Russakovsky, J. Deng, H. Su, J. Krause, S. Satheesh, S. Ma, Z. Huang, A. Karpathy, A. Khosla, M. Bernstein, A. C. Berg, and L. Fei-Fei, "ImageNet Large Scale Visual Recognition Challenge," *International Journal of Computer Vision (IJCV)*, vol. 115, no. 3, pp. 211–252, 2015.
- [22] P. Wang, Y. Gan, P. Shui, F. Yu, Y. Zhang, S. Chen, and Z. Sun, "3d shape segmentation via shape fully convolutional networks," *Computers & Graphics*, vol. 76, pp. 182–192, 2018.
- [23] L. Yi, L. Shao, M. Savva, H. Huang, Y. Zhou, Q. Wang, B. Graham, M. Engelcke, R. Klotz, V. Lempitsky *et al.*, "Large-scale 3d shape reconstruction and segmentation from shapenet core55," *arXiv preprint arXiv:1710.06104*, 2017.
- [24] Q. Meng, W. Wang, T. Zhou, J. Shen, Y. Jia, and L. Van Gool, "Towards a weakly supervised framework for 3d point cloud object detection and annotation," *IEEE Transactions on Pattern Analysis and Machine Intelligence*, 2021.
- [25] Y. Chen, V. T. Hu, E. Gavves, T. Mensink, P. Mettes, P. Yang, and C. G. Snoek, "Pointmixup: Augmentation for point clouds," in *Computer Vision—ECCV 2020: 16th European Conference, Glasgow, UK, August 23–28, 2020, Proceedings, Part III 16*. Springer, 2020, pp. 330–345.
- [26] D. Maturana and S. Scherer, "Voxnet: A 3d convolutional neural network for real-time object recognition," in *2015 IEEE/RSJ International Conference on Intelligent Robots and Systems (IROS)*. IEEE, 2015, pp. 922–928.
- [27] H. Su, S. Maji, E. Kalogerakis, and E. Learned-Miller, "Multi-view convolutional neural networks for 3d shape recognition," in *Proceedings of the IEEE international conference on computer vision*, 2015, pp. 945–953.
- [28] Z. Li, H. Wang, and J. Li, "Auto-mvcnn: Neural architecture search for multi-view 3d shape recognition," *arXiv preprint arXiv:2012.05493*, 2020.
- [29] Y. Zhang, Z. Zhou, P. David, X. Yue, Z. Xi, B. Gong, and H. Foroosh, "Polarnet: An improved grid representation for online lidar point clouds semantic segmentation," in *Proceedings of the IEEE/CVF Conference on Computer Vision and Pattern Recognition*, 2020, pp. 9601–9610.
- [30] C. R. Qi, H. Su, K. Mo, and L. J. Guibas, "Pointnet: Deep learning on point sets for 3d classification and segmentation," in *Proceedings of the IEEE conference on computer vision and pattern recognition*, 2017, pp. 652–660.
- [31] C. R. Qi, L. Yi, H. Su, and L. J. Guibas, "Pointnet++: Deep hierarchical feature learning on point sets in a metric space," *arXiv preprint arXiv:1706.02413*, 2017.
- [32] Q. Hu, B. Yang, L. Xie, S. Rosa, Y. Guo, Z. Wang, N. Trigoni, and A. Markham, "Randla-net: Efficient semantic segmentation of large-scale point clouds," in *Proceedings of the IEEE/CVF Conference on Computer Vision and Pattern Recognition*, 2020, pp. 11 108–11 117.
- [33] Y. Wang, Y. Sun, Z. Liu, S. E. Sarma, M. M. Bronstein, and J. M. Solomon, "Dynamic graph cnn for learning on point clouds," *Acm Transactions On Graphics (tog)*, vol. 38, no. 5, pp. 1–12, 2019.
- [34] H. Thomas, C. R. Qi, J.-E. Deschaud, B. Marcotegui, F. Goulette, and L. J. Guibas, "Kpconv: Flexible and deformable convolution for point clouds," in *Proceedings of the IEEE/CVF International Conference on Computer Vision*, 2019, pp. 6411–6420.
- [35] M. Xu, R. Ding, H. Zhao, and X. Qi, "Paconv: Position adaptive convolution with dynamic kernel assembling on point clouds," in *Proceedings of the IEEE/CVF Conference on Computer Vision and Pattern Recognition*, 2021, pp. 3173–3182.
- [36] H. Zhao, L. Jiang, J. Jia, P. Torr, and V. Koltun, "Point transformer," *arXiv preprint arXiv:2012.09164*, 2020.
- [37] M.-H. Guo, J.-X. Cai, Z.-N. Liu, T.-J. Mu, R. R. Martin, and S.-M. Hu, "Pct: Point cloud transformer," *arXiv preprint arXiv:2012.09688*, 2020.
- [38] S. Gidaris, P. Singh, and N. Komodakis, "Unsupervised representation learning by predicting image rotations," *arXiv preprint arXiv:1803.07728*, 2018.
- [39] M. Noroozi and P. Favaro, "Unsupervised learning of visual representations by solving jigsaw puzzles," in *European conference on computer vision*. Springer, 2016, pp. 69–84.
- [40] R. Zhang, P. Isola, and A. A. Efros, "Colorful image colorization," in *European conference on computer vision*. Springer, 2016, pp. 649–666.
- [41] C. Ledig, L. Theis, F. Huszar, J. Caballero, A. Cunningham, A. Acosta, A. Aitken, A. Tejani, J. Totz, and Z. Wang, "Photo-realistic single image super-resolution using a generative adversarial network," in *IEEE Computer Society*, 2016.
- [42] D. Pathak, P. Krahenbuhl, J. Donahue, T. Darrell, and A. A. Efros, "Context encoders: Feature learning by inpainting," *IEEE*, 2016.
- [43] I. J. Goodfellow, J. Pouget-Abadie, M. Mirza, B. Xu, D. Warde-Farley, S. Ozair, A. Courville, and Y. Bengio, "Generative adversarial networks," *Advances in Neural Information Processing Systems*, vol. 3, pp. 2672–2680, 2014.
- [44] J. Y. Zhu, T. Park, P. Isola, and A. A. Efros, "Unpaired image-to-image translation using cycle-consistent adversarial networks," *IEEE*, 2017.
- [45] A. v. d. Oord, Y. Li, and O. Vinyals, "Representation learning with contrastive predictive coding," *arXiv preprint arXiv:1807.03748*, 2018.
- [46] T. Chen, S. Kornblith, M. Norouzi, and G. Hinton, "A simple framework for contrastive learning of visual representations," in *International conference on machine learning*. PMLR, 2020, pp. 1597–1607.
- [47] K. He, H. Fan, Y. Wu, S. Xie, and R. Girshick, "Momentum contrast for unsupervised visual representation learning," in *Proceedings of the*

*IEEE/CVF Conference on Computer Vision and Pattern Recognition*, 2020, pp. 9729–9738.

- [48] T. Han, W. Xie, and A. Zisserman, “Self-supervised co-training for video representation learning,” *arXiv preprint arXiv:2010.09709*, 2020.
- [49] J.-B. Grill, F. Strub, F. Alché, C. Tallec, P. H. Richemond, E. Buchatskaya, C. Doersch, B. A. Pires, Z. D. Guo, M. G. Azar *et al.*, “Bootstrap your own latent: A new approach to self-supervised learning,” *arXiv preprint arXiv:2006.07733*, 2020.
- [50] J. Zbontar, L. Jing, I. Misra, Y. LeCun, and S. Deny, “Barlow twins: Self-supervised learning via redundancy reduction,” *arXiv preprint arXiv:2103.03230*, 2021.
- [51] Z. Zhang, R. Girdhar, A. Joulin, and I. Misra, “Self-supervised pretraining of 3d features on any point-cloud,” *arXiv preprint arXiv:2101.02691*, 2021.
- [52] V. Nair and G. E. Hinton, “Rectified linear units improve restricted boltzmann machines,” in *Icml*, 2010.
- [53] R. Hadsell, S. Chopra, and Y. Lecun, “Dimensionality reduction by learning an invariant mapping,” in *2006 IEEE Computer Society Conference on Computer Vision and Pattern Recognition (CVPR’06)*, 2006.
- [54] Z. Zheng, L. Zheng, M. Garrett, Y. Yang, M. Xu, and Y.-D. Shen, “Dual-path convolutional image-text embeddings with instance loss,” *ACM Transactions on Multimedia Computing, Communications, and Applications (TOMM)*, vol. 16, no. 2, pp. 1–23, 2020, doi:[10.1145/3383184](https://doi.org/10.1145/3383184).
- [55] C. Wang, B. Samari, and K. Siddiqi, “Local spectral graph convolution for point set feature learning,” in *ECCV*, 2018.
- [56] M. Atzmon, H. Maron, and Y. Lipman, “Point convolutional neural networks by extension operators,” *ACM Transactions on Graphics*, 2018.
- [57] Z. Zheng and Y. Yang, “Parameter-efficient person re-identification in the 3d space,” *arXiv preprint arXiv:2006.04569*, 2020.
- [58] A. X. Chang, T. Funkhouser, L. Guibas, P. Hanrahan, Q. Huang, Z. Li, S. Savarese, M. Savva, S. Song, H. Su, J. Xiao, L. Yi, and F. Yu, “ShapeNet: An Information-Rich 3D Model Repository,” Stanford University — Princeton University — Toyota Technological Institute at Chicago, Tech. Rep. arXiv:1512.03012 [cs.GR], 2015.
- [59] I. Loshchilov and F. Hutter, “Sgdr: Stochastic gradient descent with warm restarts,” in *ICLR 2017 (5th International Conference on Learning Representations)*, 2016.
- [60] L. Van der Maaten and G. Hinton, “Visualizing data using t-sne.” *Journal of machine learning research*, vol. 9, no. 11, 2008.



**Yi Yang** received the Ph.D. degree in computer science from Zhejiang University, Hangzhou, China, in 2010. He is currently a professor with University of Technology Sydney, Australia. He was a Post-Doctoral Research with the School of Computer Science, Carnegie Mellon University, Pittsburgh, PA, USA. His current research interest includes machine learning and its applications to multimedia content analysis and computer vision, such as multimedia indexing and retrieval, video analysis and video semantics understanding.



**Chao Sun** received the B.E. degree in software engineering from Zhejiang University, China, in 2021. He is currently a master student with the School of Computer Science at Zhejiang University, China. His current research interests include point cloud classification and segmentation.



**Zhedong Zheng** received the B.S. degree in computer science from Fudan University, China, in 2016. He is currently a Ph.D. student with the School of Computer Science at University of Technology Sydney, Australia. He was an intern at Nvidia Research (2018) and Baidu Research (2020). His research interests include robust learning for image retrieval, generative learning for data augmentation, and unsupervised domain adaptation.